ELECTROCHEMICAL ENERGY STORAGE DEVICES

By

Arlin Alvarado Hernandez, Guanglian Li, Sylvia Nguyen, Fouche Smith, and Timur Takhtaganov

IMA Preprint Series #2433

(August 2014)

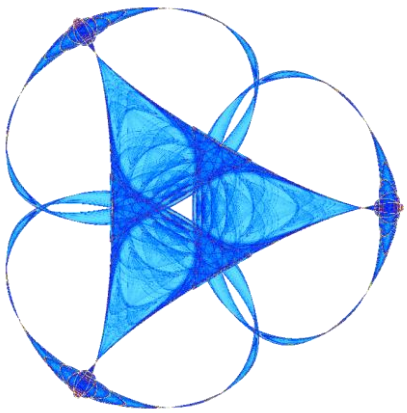

INSTITUTE FOR MATHEMATICS AND ITS APPLICATIONS
UNIVERSITY OF MINNESOTA
400 Lind Hall
207 Church Street S.E.
Minneapolis, Minnesota 55455-0436
Phone: 612-624-6066 Fax: 612-626-7370
URL: http://www.ima.umn.edu

Electrochemical Energy Storage Devices

Arlin Alvarado Hernandez [*]
University of Puerto Rico

Guanglian Li [†]
Texas A & M University

Sylvia Nguyen [‡]
University of Guelph

Fouche Smith [§]
University of Kentucky

Timur Takhtaganov [¶]
Rice University

Mentor
Dr. Rajeswari Chandrasekaran[1]
Research and Advanced Engineering
Ford Motor Company, MI.

Abstract

In this project, we obtained a better understanding of modeling of lithium-ion batteries including the optimization of porosity and thickness of the positive electrode to maximize specific energy and specific power, the capacity loss during storage due to SEI growth formed between the negative electrode and electrolyte, and the dendrite growth in lithium polymer systems during galvanostatic charging which can pose a safety concern by rederiving and reproducing results from the literature [1], [2], [3] and [4].

1 Introduction

Lithium-ion batteries are used in many applications from electronic devices to vehicles. Since it is the lightest metal and is highly electropositive, lithium-ion batteries have higher specific energy (Wh/ kg) and specific power (W/kg) than lead acid batteries and nickelmetal hydride batteries[10]. The specific energy and the specific power serve as an indicator of the range and acceleration of a vehicle, respectively.

A lithium-ion cell consists of a composite negative electrode and a composite positive electrode. They are divided by a porous separator through which lithium ions transport from one electrode to another. The porous composite electrodes consist of active material, binder and conductive carbon (if needed). The pores are filled with electrolyte (Li salt such as LiPF6 in organic solvent). The separator prevents electronic contact between the positive and the negative electrodes and thus prevents shorting. The negative composite electrode is usually coated on to a Cu current collector

[*]email: arlin.alvarado@upr.edu
[†]email: lotusli0707@gmail.com
[‡]email: snguyen@uoguelph.ca
[§]email: fouche.s@uky.edu
[¶]email: tat3@rice.edu
[1]rchand35@ford.com

and the positive on to a Al current collector. These current collectors are connected to a load, such as a car. When the battery discharges, electrons from the negative electrode move through the external circuit (i.e. from the Cu current collector, to the load, and then to the Al current collector of the positive electrode). Simultaneously, the lithium-ions from the negative electrode move through the separator and into the positive electrode. Electrons react with lithium ions and solid lithium intercalates into the active materials in the composite electrodes. This changes the composition of the electrodes.
Our report is arranged as follows. In section 2 and 3, we construct the models for specific energy, capacity, and specific power to obtain the optimal porosity and thickness of the ohmically limited porous positive electrode. In section 4, we will show that the thickness of the SEI as well as the capacity loss are linearly dependent on the square root of the time. In section 5, we will obtain the model for dendrite growth, and research the factors, such as current density and interelectrode distance, that can influence the growth of dendrites. In section 6, we summarize our main results of this project. In section 8, we display most of the MATLAB codes we developed to obtain our results, and in section 9, we have provided the list of symbols used in the report.

2 Galvanostatic Discharge in Ohmically Limited Porous Electrodes

Maximizing the capacity (Q) of the lithium ion battery is desired. To acquire this, a galvanostatic discharge of an electrode is considered here. It is also assumed that voltage losses are attributed to only ohmic resistances. From these conditions, the reaction zone is very narrow. Furthermore, the highly porous separator and the positive electrode will only be considered. The conductivity of the solid matrix is assumed to be unaffected by the reactions.

2.1 Effective Capacity

The following is the equation for effective capacity and the theoretical capacity, respectively

$$Q = it, \tag{1}$$

$$Q_T(L) = qL. \tag{2}$$

Using Ohm's law (Eqn. (3)) and the expression for resistance (Eqn. (4)), Eqn.(5) is derived from Eqn.(1). Eqn.(5) expresses capacity as a function of electrode thickness.

$$\Delta V = iR_{(i,t)}, \tag{3}$$

$$R_{(i,t)} = \frac{L_s}{\kappa_s} + \frac{L}{\kappa+\sigma} + \frac{it}{q(\kappa+\sigma)}\left[\left(\frac{\sigma}{\kappa'} + \frac{\kappa}{\sigma'}\right)(1+f) - 1\right], \tag{4}$$

yields

$$Q(L) = \frac{(\kappa+\sigma)\left(\frac{\Delta V}{i} - \frac{L}{\kappa+\sigma} - \frac{L_s}{\kappa_s}\right)q}{\left(\frac{\sigma}{\kappa'} + \frac{\kappa}{\sigma'}\right)(1+f) - 1}. \tag{5}$$

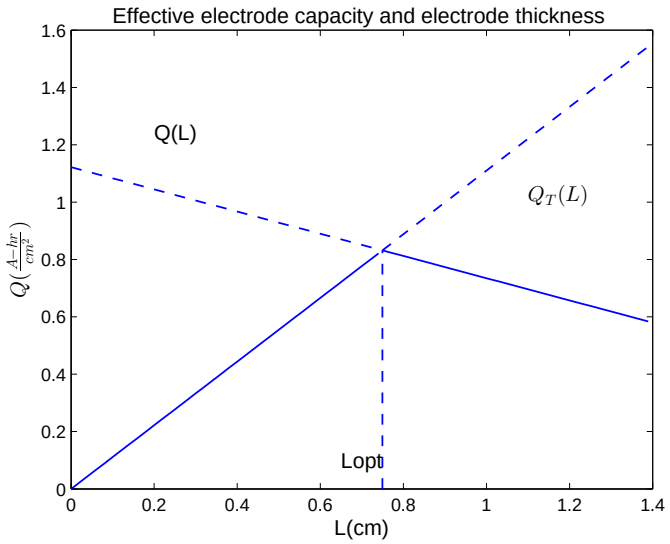

Figure 1: Effective electrode capacity and electrode thickness.

2.2 Thickness of the Electrode

Equating Equations (2) and (5) and solving for L will yield the optimal electrode thickness. Fig.1 shows the effective electrode capacity plotted as a function of electrode thickness using the two Eqns. (1) and (2) as labelled. Their intersection is the optimal electrode thickness (L_{opt}). It provides the relation between Q and Q_T, with the dashline denoting unattainable points because of no more active material in the electrode or exceeding the allowable potential loss.

2.3 Optimal Porosity

Once the thickness has been chosen, the optimal porosity can be determined. The following are empirical equations used to convert Eqn. (5) from a function of electrode thickness to a function of porosity:

$$\begin{aligned} \kappa &= \kappa_0 \epsilon^n, \\ \kappa' &= \kappa_0 \epsilon_f^n, \\ \sigma &= \sigma_0 (1-\epsilon)^n, \\ \sigma' &= \sigma_0' (1-\epsilon_f)^n, \\ q &= q_0 (1-\epsilon), \\ \epsilon_f &= 1 - \frac{1-\epsilon}{B}. \end{aligned} \tag{6}$$

Substituting these empirical equations into Eqn. (5) yields

$$Q(\epsilon) = \frac{q_0(1-\epsilon)(\kappa_0\epsilon^n + \sigma_0(1-\epsilon)^n)\left(\frac{\Delta V}{i} - \frac{L_s}{\kappa_s}\right)}{\left[\frac{\sigma_0(1-\epsilon)^n}{\kappa_0\left(1-\frac{1-\epsilon}{B}\right)^n} + \frac{\kappa_0\epsilon^n}{\sigma_0'\left(\frac{1-\epsilon}{B}\right)^n}\right](1+f)}. \tag{7}$$

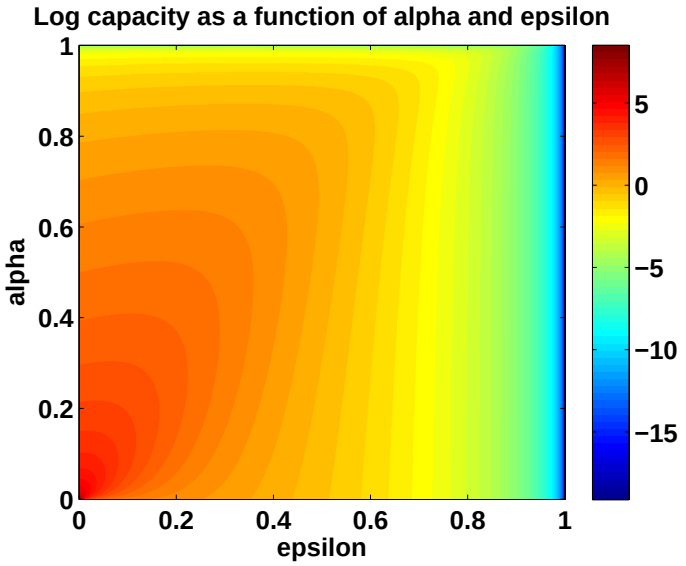

Figure 2: Electrode capacity for various electrode thickness and porosity.

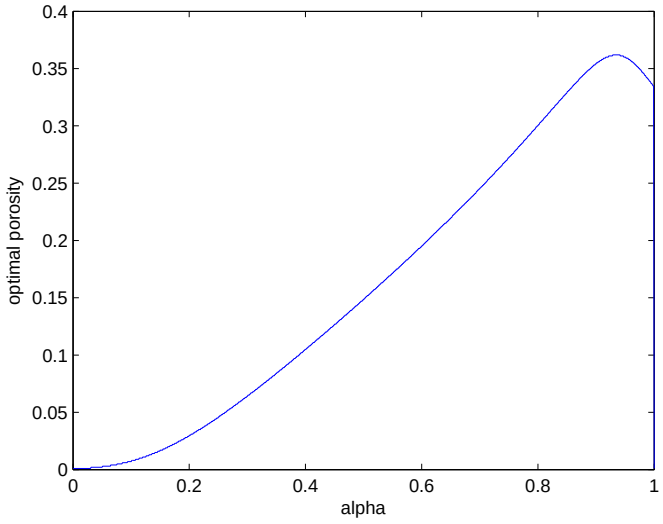

Figure 3: Optimal electrode thickness and porosities.

Using Eqn. (7), a contour map can be made to plot the capacity as a function of porosity and the ratio of the bulk conductivities of the electrolyte and the solid matrix denoted as α, and $\alpha = \frac{\sigma_0}{\sigma_0+\kappa_0}$. This map is shown in Fig. 2. It shows that for a smaller α value, capacity is maximized at lower porosities.

Fig. 2 shows the effective capacity as a function of ratio of solid conductivity α and porosity ϵ. In this figure, the capacity increases from blue to red in the color scale. Therefore, to maximize capacity, the porosity should be relatively small and α should be relatively small as well. This

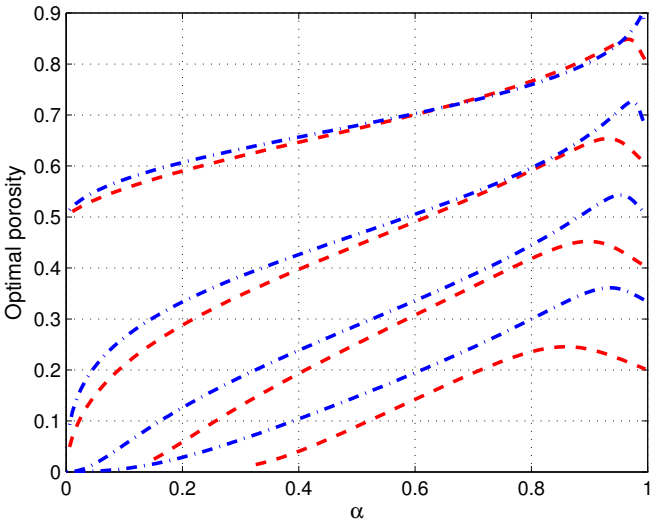

Figure 4: Dependence of the optimum porosity on the relative conductivities of the bulk matrix and solution phases, with red dotted line $n = 1.5$, and blue dotted line $n = 2$.

implies that the conductivity of the electrolyte should be large. For a given α we determine the optimal porosity at peak capacity.

For Figs. 2 and 3, the plots are for $B = 1$ and $n = 1.5$. B is the parameter that takes into account the volumetric changes within the battery. n is the tortuosity. Tortuosity is a measure of how winding a path is for the transport of the charged species (mainly lithium ions) through the porous media within the cell. As n approaches infinity, the path becomes more winding. Here, only n between 1 and 3 are considered.

Figs.4 and 5 are plots of the dependence of the optimum porosity on α with varying B and n. The optimal porosities are varied using different ratios of the bulk conductivities of the unreacted and reacted components of the solid matrix.

3 Optimization of Porosity and Thickness for discharge times

In the analysis of the previous section the capacity of the electrode was maximized as a function of the electrode thickness and the porosity. Now we wish to maximize the specific energy, E as a function of porosity and electrode thickness for various discharging time. Maximizing the specific energy is advantageous because it takes into account the overall mass of the system. The discharge time gives insight into the particular application of the vehicle.

3.1 Specific Energy

The assumptions from the previous section will be preserved. Activation and concentration over-potentials are considered negligible relative to ohmic resistance. Also the current distribution, i, is

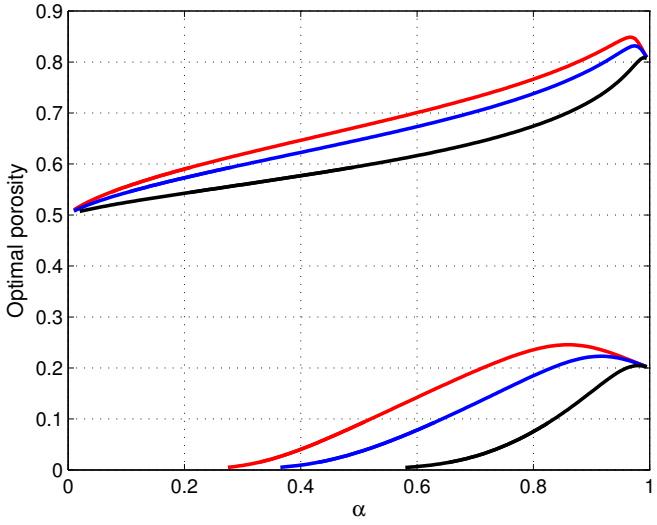

Figure 5: Relation between porosity and conductivity of the bulk matrix and solution phase. Solid phase conductivity ratio between discharged and charged state: red:1; blue: 0.5; and black: 0.1.

non-uniform. Combining these results, the cell potential at any given time becomes

$$V = U - \frac{L_s}{\kappa_s} i - \frac{i^2 t}{\kappa(1-\epsilon)q_+}, \tag{8}$$

the energy per unit separator area becomes

$$E = \int V i dt = (U - \frac{L_s}{\kappa_s i}) i t_d - \frac{i^3 t_d^2}{2\kappa(1-\epsilon)q_+}. \tag{9}$$

To rescale the problem, we introduce the following dimensionless parameters. The dimensionless current becomes, $I = \frac{iL_s}{\kappa_s U}$, and the dimensionless discharge time becomes, $T = \frac{U\kappa_s t_d}{q_+ L_s^2}$. The current that maximizes energy is

$$I_{opt}^1 = \frac{1}{1 + (1 + \frac{T\kappa_s}{2\kappa(1-\epsilon)})^{1/2}}. \tag{10}$$

However, there are two constraints to consider. Once the electrode has completely discharged, the cell potential should not drop below the cut-off voltage to preserve the lifespan of the battery. This forces

$$I_{opt}^2 \leq \frac{2(1 - \frac{V_c}{U})}{1 + (1 + \frac{4(U-V_c)t_d\kappa_s^2}{2\kappa(1-\epsilon)q_+ L_s^2})^{1/2}}. \tag{11}$$

Also the capacity of the positive electrode must not be exceeded, so

$$I_{opt}^3 \leq \frac{L_+}{L_s} \frac{(1-\epsilon)}{T}, \tag{12}$$

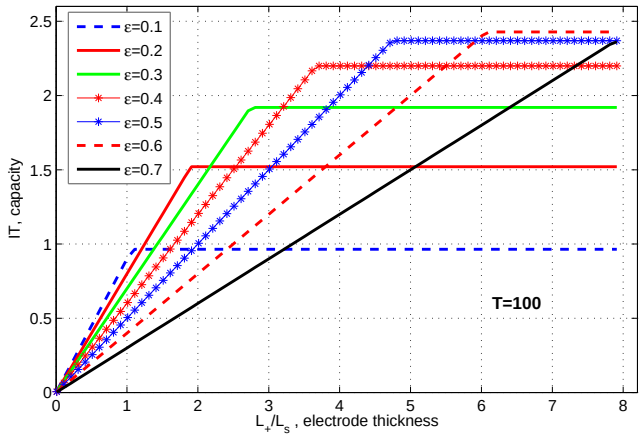

Figure 6: Electrode capacity for various electrode thickness and porosity.

the optimal current, $I_{opt} = \min(I^1_{opt}, I^2_{opt}, I^3_{opt})$. The total mass per unit separator area becomes

$$M = \rho_r L_r + \rho_s L_s + [\rho_- q_+ (1-\epsilon)/q_- + \epsilon\rho_s + (1-\epsilon)\rho_s]L_+. \tag{13}$$

Finally the dimensionless specific energy now becomes

$$\bar{E} = \frac{(1-I)IT - \frac{I^3T^2}{2\epsilon^{1.5}(1-\epsilon)}}{\frac{\rho_r L_r}{\rho s L_s} + 1 + \frac{L_+}{L_s}[\epsilon + \frac{\rho_+}{\rho_s}(1-\epsilon)]}. \tag{14}$$

3.2 Optimum Specific Energy vs. Optimal Capacity

First we consider the capacity as a function of dimensionless electrode thickness for fixed discharge time. Fig. 6 depicts the capacity of the system as a function of electrode thickness for fixed a discharge time of $T = 100$ at various values of ϵ. In Fig. 6, we consider the relation between the capacity and electrode thickness for fixed ϵ. For relatively small electrode thickness, the capacity is directly proportional to the thickness of the system. In this case $I_{opt} = I^1_{opt}$. Once the electrode thickness reaches a certain threshold value, the capacity remains constant. This implies that one of our constraints have been met. So $I_{opt} = \min(I^2_{opt}, I^3_{opt})$. By inspection the optimal porosity and thickness predicted by the capacity is .6 and 6 respectively when $T = 100$.
Next we consider the specific energy as a function of electrode thickness. In Fig.7, we depict the specific energy of the system as a function of electrode thickness for a fixed discharge time of $T = 100$ at various values of ϵ. The optimal porosity and thickness predicted by the specific energy is 0.227 and 1.95 when $T = 100$. In this scenario the specific energy diminishes the optimal porosity and thickness by about 67%. The specific energy predicts smaller optimal porosity and thickness because it takes into account the mass of the electrode.

3.3 Specific Energy vs. Average Specific Power

Fig.8 depicts the relation between specific energy and average specific power and is called a Ragone plot. In the context of electric vehicle applications, the figure can be thought of as the range against

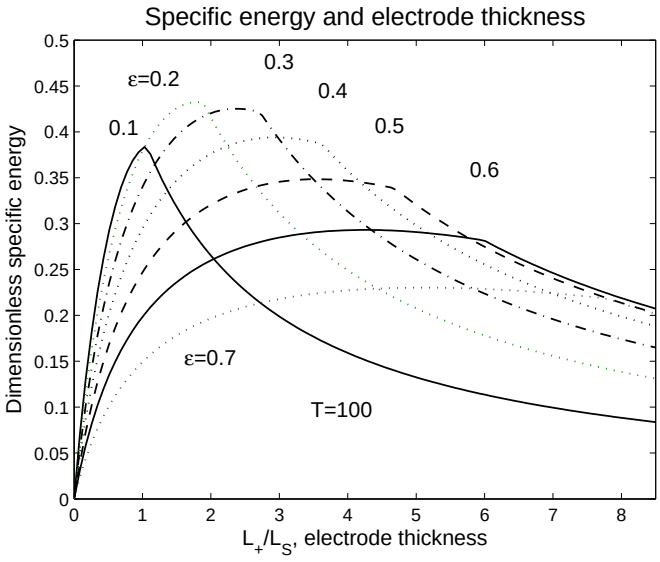

Figure 7: Specific energy for various electrode thickness and porosities.

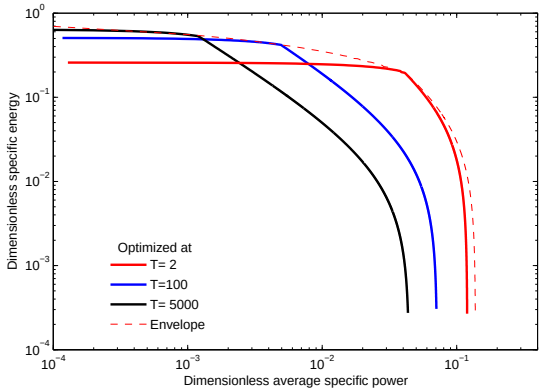

Figure 8: Specific energy vs. specific power.

the acceleration. For electrode designed for a discharge time of $T = 2$, the maximum specific energy is relatively small. However, even as the average power gets large, the specific energy remains high. This suggests a small discharge time is more suited for high power applications. For a discharge time of $T = 5000$, the maximum specific energy is relatively large. However, as the average specific power obtained remains high, the specific energy delivered decreases relatively fast. This suggests that thicker electrodes are most suitable for continuous low power to moderate activities that need to be sustained for a long time.

4 Solvent Diffusion Model for Aging of Lithium-Ion Battery Cells

Solid-electrolyte interface (SEI) in lithium-ion batteries is the passive layer that is formed over the negative electrode. Solvent reduction contributes to the formation of SEI and leads to capacity

loss. This irreversible capacity loss happens during the first few charges of the battery and is necessary, because isolating negative electrode from the electrolyte minimizes further reduction of electrolyte components. "Good" electrolytes produce thin and dense SEI films that have low solvent permeability and are able to withstand volume changes due to lithium intercalation-deintercalation. "Poor" electrolytes lead to porous SEI films that may permit continuing reduction of solvent, thus, reducing the capacity of the battery.
Here we study simple model of formation of SEI [3].

4.1 Model

Assumptions.

- The reaction of one solvent component (S) dominates. This component undergoes two-electron reduction at the carbon-SEI interface via

$$S + 2e^- + 2Li^+ \rightarrow P; \tag{15}$$

- Within the SEI phase, component S is the only mobile component and has a constant effective diffusivity (D_S);
- S is dilute within the SEI so that $c_S \ll c_P$;
- Electrons and lithium cations are available in excess at the carbon-SEI interface;
- c_P is constant and a reference frame in which the SEI/electrolyte interface is stationary, the flux of P is zero and the differential mass balance for P is satisfied identically.

Using similarity transformation we have the following dimensionless diffusion equation for the concentration of S derived from the differential mass balance ,

$$\frac{d^2c_S}{du^2} + 2u\frac{dc_S}{du} = 0 \tag{16}$$

$$c_S = 0, \text{ at } u = \lambda, \tag{17}$$

$$c_S = c_{eq}, \text{ at } u = 0, \tag{18}$$

where $u = \frac{z}{\sqrt{4D_S t}}$ and $\lambda = \frac{L(t)}{\sqrt{4D_S t}}$.
Using results in [6] and [7], we obtain
The solution of this problem is given by

$$c_S(z,t) = c_{eq}\left(1 - \frac{\text{erf}(u)}{\text{erf}(\lambda}\right) \tag{19}$$

where λ may be found from the solution of

$$\lambda = \frac{c_{eq}}{\sqrt{\pi c_p}}\frac{\exp -\lambda^2}{erf(\lambda)} \tag{20}$$

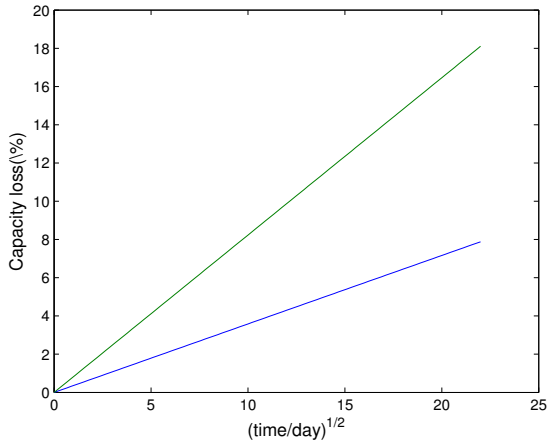

(a) Capacity loss x with respect to t

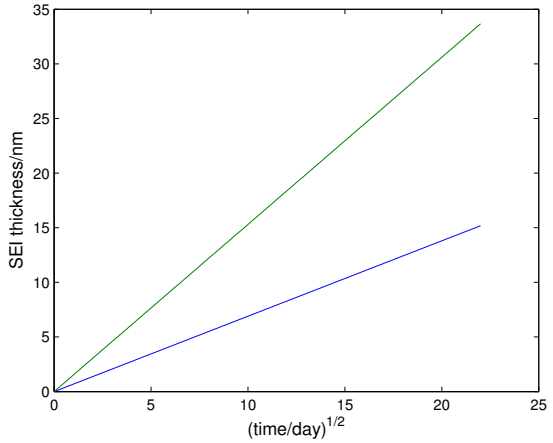

(b) Capacity loss x with respect to t

Figure 9: Capacity loss x and SEI thickness L with respect to $\sqrt{t}$

and the SEI thickness ($L(t)$) and fractional capacity loss ($x(t)$) are given by

$$L(t) = 2\lambda\sqrt{D_S t}, \tag{21}$$

$$x(t) = \frac{2Z_p c_p A_{anode}\lambda}{N_0}\sqrt{D_S t}. \tag{22}$$

In the simulation we use Eqn. (21) and (22) to get the relation between the capacity loss(x) and SEI thickness L with respect to time(t) in Fig. 9. From Fig. 9, we observe the linear dependence of the capacity loss on the square root of the time for HE prototype cells stored at temperatures of 30 and 60°C, respectively. Similarly, the dependence of the SEI thickness on the square root of the time is also linear. In Fig. 10, we show the remaining capacity in a time span of 100 days.

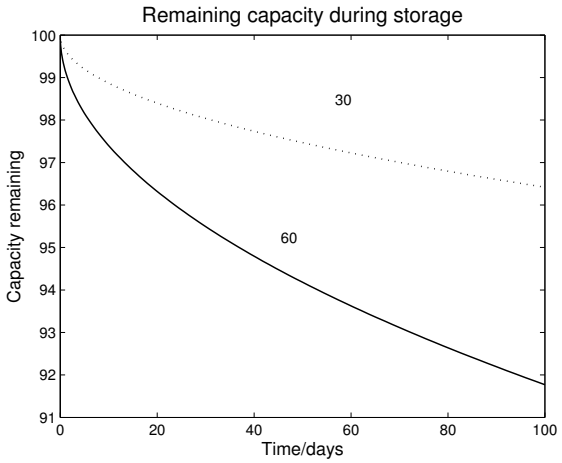

Figure 10: Capacity remaining with respect to time t.

5 Dendrite Growth in Li/Polymer Systems

Although lithium has higher specific capacity than graphite for lithium insertion, it is not commercially used for most applications due to the problem of dendrite growth. Better understanding of this issue can lead to mitigation efforts. Therefore, we seek to model the dendrite growth in a lithium polymer cell during galvanostatic charging. This model is surface-energy controlled and it takes into account the effect of dendrite tip curvature into the kinetics of its dendrite growth. [4]

5.1 Objective

We want to simulate the dendrite growth in a parallel-electrode lithium/polymer cell during galvanostatic charging.

5.2 Model

Assumptions.

- The electrolyte behaves ideally, i.e., the solution is relatively dilute and the activity coefficients are unity.
- Material and transport properties are treated as constant with respect to concentration.
- The cell is presumed to be isothermal.
- A typical charge cycle is assumed to last three hours.

Firstly, we need to obtain concentration and potential profiles for a binary electrolyte. Given an initial bulk concentration of lithium salt (c_b) in the separator we need to solve the following transient diffusion equation for overall salt concentration (c),

$$\frac{\partial c}{\partial t} = D\frac{\partial^2 c}{\partial y^2}, \tag{23}$$

where the Laplacian is reduced to one dimension, and y denotes the direction from negative electrode to positive, perpendicular to both of them. This equation is subject to boundary conditions,

$$i = -\frac{DF}{(1-t_+^0)}\frac{\partial c}{\partial y}\bigg|_{y=0}, \tag{24}$$

$$\frac{1}{L}\int_0^L c(y,t)dy = c_b, \tag{25}$$

$$c = c_b \text{ at } t = 0. \tag{26}$$

Where F is Faraday's constant and t_+^0 is the cation transference number.
These equations can be nondimensionalized using change of variables of the following form,

$$\xi = \frac{y}{L}, \tag{27}$$

$$\tau = \frac{Dt}{L^2}, \tag{28}$$

$$\theta = \frac{(c-c_b)DF}{(1-t_+^0)iL}. \tag{29}$$

Then the problem can be transformed to the following type,

$$\frac{\partial\theta}{\partial\tau} = \frac{\partial^2\theta}{\partial\xi^2}, \tag{30}$$

$$\frac{\partial\theta}{\partial\xi}\bigg|_{\xi=0} = -1 \qquad , \tag{31}$$

$$\int_0^1 \theta_T(\tau,\xi)d\xi = 0, \tag{32}$$

$$\theta = 0 \text{ at } \tau = 0. \tag{33}$$

Now we are going to solve problem (30) by decomposing θ as follows,

$$\theta(\xi,\tau) = \theta_{SS}(\xi) + \theta_T(\xi,\tau), \tag{34}$$

and the steady-state solution (θ_{SS}) is found by simple integration, while transient solution (θ_T) is found using separation of variables and Fourier series. We arrive at the following form,

$$\theta = -\xi + \frac{1}{2} - 4\sum_{k=1}^{\infty}\frac{1}{(2k-1)^2\pi^2}e^{-(2k-1)^2\pi^2\tau}\times\cos[(2k-1)\pi\xi], \tag{35}$$

Resulting concentration profile is depicted in Fig. 11.
To find the potential profile we use Butler-Volmer type expression,

$$\frac{i}{F} = \kappa_a\exp\left(\frac{\alpha_a F}{RT}\Phi\right) - \kappa_c c\exp\left(\frac{-\alpha_c F}{RT}\Phi\right) \tag{36}$$

We assume that potential relative to the cathode can be written as the sum of open-circuit overpotential (OCP) and a surface overpotential, i.e.,

$$\Phi = V_0 + \eta_s \tag{37}$$

When the current is zero, the OCP is achieved. We, therefore, can solve for V_0:

$$V_0 = \frac{RT}{(\alpha_a + \alpha_c)F} \ln\left(\frac{\kappa_c c}{\kappa_a}\right) \tag{38}$$

Then assuming the transfer coefficients sum to unity we obtain,

$$\frac{i}{F} = \kappa_a^{\alpha_c}(\kappa_c c)^{\alpha_a}\left[\exp\left(\frac{\alpha_a F}{RT}\eta_s\right) - \exp\left(\frac{-\alpha_c F}{RT}\eta_s\right)\right] \tag{39}$$

Using Eqn. (39), we define exchange current density as

$$i_0 = \kappa_a^{\alpha_c}(\kappa_c c)^{\alpha_a} = i_{0,ref}\left(\frac{c}{c_{ref}}\right)^{\alpha_a} \tag{40}$$

Assuming $\alpha_a = \alpha_c = 1/2$ we obtain analytic expression for the surface overpotential,

$$\eta_s = \frac{2RT}{F}\sinh^{-1}\left[\frac{1}{2}\left(\frac{i}{i_{0,ref}}\right)\left(\frac{c_{ref}}{c}\right)^{1/2}\right] \tag{41}$$

Finally, with the overpotential as a boundary condition, we use the integrated form of modified Ohm's law to find the instantaneous potential as

$$\Phi_3(y,t) = \eta_s - \frac{i}{\Lambda}\int_0^y \frac{1}{c}\mathrm{d}y + \frac{RT}{F}(1-2t_+^0)\ln\left[\frac{c(y,t)}{c(0,t)}\right] \tag{42}$$

Here Λ is the equivalent conductance of the electrolyte and is given by

$$\Lambda = \frac{F^2 D}{2t_+^0(1-t_+^0)RT} \tag{43}$$

Fig. 12 shows the potential in the separator, i.e. the profile for Eqn.(42).
Now we assume that there is single dendrite protruding from the cathode, sufficiently far apart form the other dendrites. We also assume that dendrite so small that it does not affect the concentration and potential in the cell. Furthermore, the growth of the dendrite does not lower the bulk concentration of lithium appreciably. The expression for the kinetics of the dendrite growth is given below.

$$\frac{i_n}{i_{0,ref}} = \frac{\exp\left(\frac{2\gamma V}{rRT}\right)\exp\left(\frac{\alpha_a F\eta}{RT}\right) - \exp\left(\frac{-\alpha_c F\eta}{RT}\right)}{\left(\frac{c_{ref}}{c_{Li^+}}\right)^{\alpha_a} + \frac{(1-t_+^0)ri_{0,ref}}{FDc_{Li^+}^{\delta'}}\exp\left(\frac{-\alpha_c F\eta}{RT}\right)}; \tag{44}$$

Notice that the dendrite radius r is a variable, but in the simulation, we choose a constant radius that maximizes the tip current i_n.
The current density at the dendrite tip i_n is related to the propagation velocity of the dendrite v_{tip} by

$$v_{tip} = \frac{i_n(c,\eta)V}{F}, \tag{45}$$

In Fig. 13, we depict the velocity v_{tip} profile as a function of distance L for fixed time t. It shows

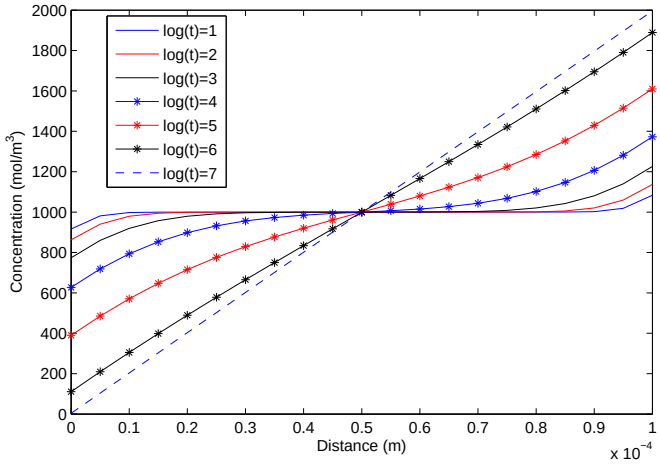

Figure 11: Concentration (θ) profile in the galvanostatic cell.

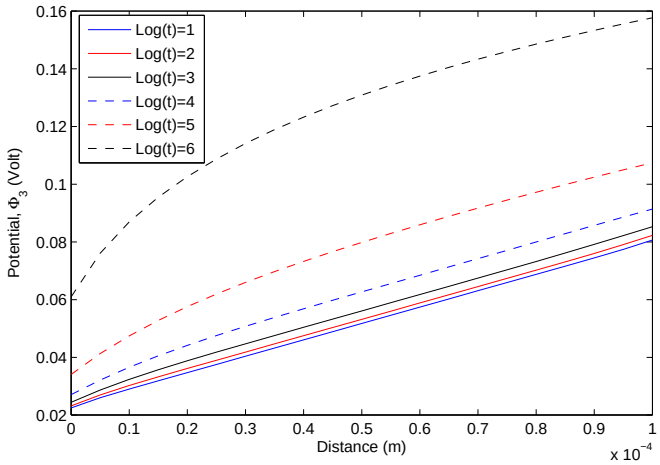

Figure 12: Potential ϕ_3 vs. distance and time in the cell.

that the relation is linear.

Finally, we can get the equations satisfied by the dendrite tip position y_{tip}. y_{tip} satisfies the following first order differential equation with the initial condition,

$$\frac{\partial y_{tip}}{\partial t} = v_{tip} = \frac{i_n(c,\eta)V}{F} \tag{46}$$
$$y_{tip} = 0 \text{ at } t = 0.$$

In Fig. 14, we show the dendrite growth y_{tip} with respect to time t. Adjusting the current density changed the shape of the dendrite growth profile (Fig. 15). Lowering the current density appeared to prolong relatively linear growth rate. From Figs. 13 and 14, we conclude that the dendrite growth accelerates both as time passed and as it moved across the cell.

Finally, we explored the effect of current density on the charge passed at failure. The results are

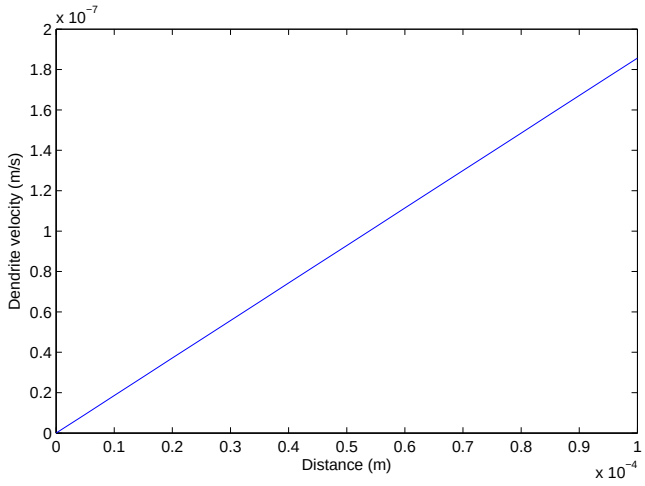

Figure 13: Dendrite velocity v_{tip} as a function of distance.

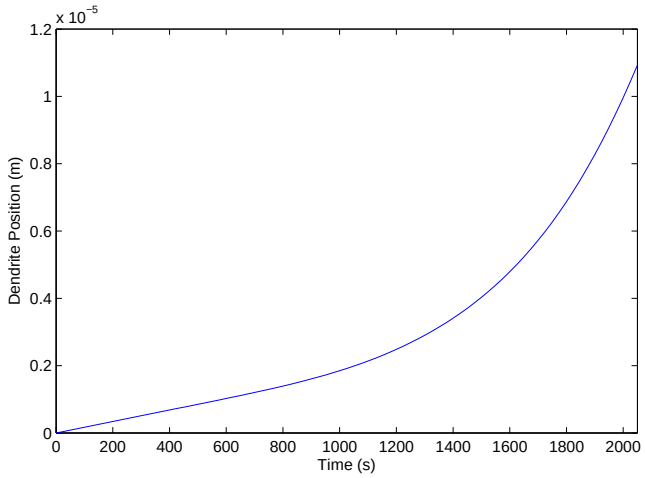

Figure 14: Dendrite position y_{tip} and time t.

depicted in Fig. 16. This figure suggests that cell fails if run above 75% of limiting current. Also, the slope of the curve suggests that lowering current density always increases the charge that can be passed before failure.

6 Conclusion

In this project, we looked at the modeling of lithium-ion batteries from different perspectives: optimization of performance, life span and safety issues.
First, we constructed the models for specific energy, capacity, and specific power to obtain the optimal porosity and thickness of the ohmically limited porous positive electrode. From our simulation results, we saw that optimal porosity depends on relative bulk conductivities of the

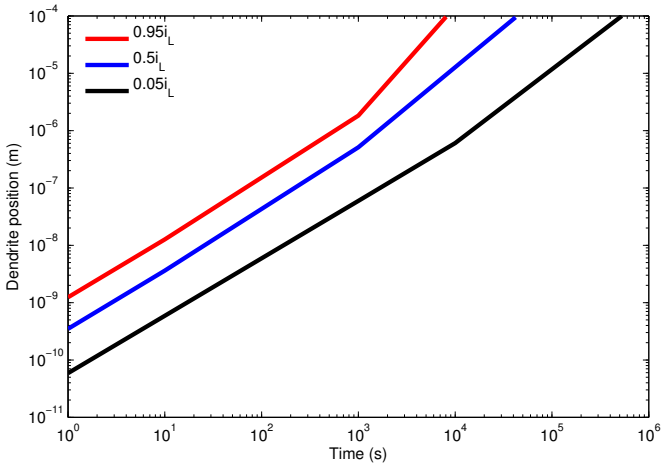

Figure 15: Dendrite growth profile shape at varying currents.

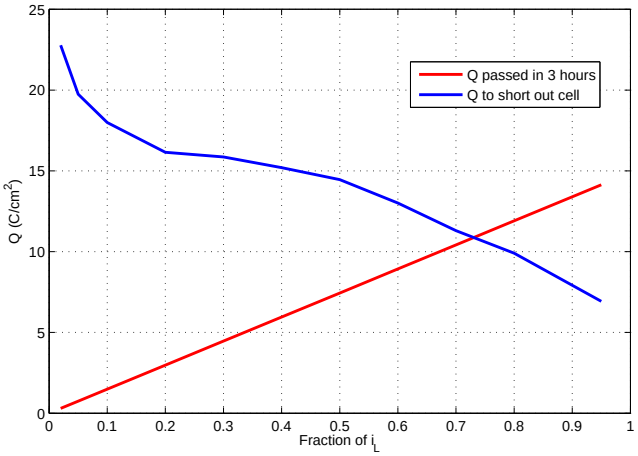

Figure 16: Charge to short out cell and charge in 3 h vs. interelectrode distance, $i = 0.95 i_L$.

solid matrix and electrolyte. It also depends on volume changes of an active material in the electrode. For example, for $B < 1$ optimal porosity is relatively large to account for increase in the volume of reacted material; for $B > 1$, it is relatively small because reacted material occupies smaller volume. Furthermore, the larger the tortuosity(n), the more important it becomes to spread the material out (larger porosity).

Next, we studied the aging of lithium-ion batteries, in particular, the growth of SEI and capacity fade associated with it. We observed that the thickness of the SEI as well as the capacity loss are linearly dependent on the square root of the time.

Finally, we obtained the model for the dendrite growth in lithium/polymer systems. We investigated the influence of different factors, such as current density and interelectrode distance, on the

growth of dendrites.

7 Acknowledgements

We would like to thank IMA and University of Minnesota for organizing this workshop. We had a great experience, learned a lot about an interesting application area and met many wonderful people.
Our special appreciation goes to our project mentor Dr. Rajeswari Chandrasekaran. Her enthusiasm, assistance and support made working on the project easy and fun.

References

[1] Tiedemann, William, and John Newman, *Maximum effective capacity in an ohmically limited porous electrode*. Journal of The Electrochemical Society 122.11 (1975): 1482-1485.

[2] John Newman, *Optimization of Porosity and Thickness of a Battery Electrode by Means of a Reaction-Zone Model*. Journal of the Electrochemical Society 142.1 (1995): 97-101.

[3] Harry J.Ploehn, Premanand Ramadass, and Ralph E. White, *Solvent diffusion model for aging of lithium-ion battery cells.* Journal of The Electrochemical Society 151.3 (2004): A456-A462. Journal of Computational Physics,230, pp. 937-955, 2011.

[4] Charles Monroe and John Newman, *Dendrite Growth in Lithium/Polymer Systems.* Journal of The Electrochemical Society 150 (10) (2003): A1377-A1384.

[5] Venkat R. Subramanian, and Ralph E. White, *New separation of variables method for composite electrodes with galvanostatic boundary conditions.* Journal of power sources 96.2 (2001): 385-395.

[6] J. C. Slattery, *Advanced Transport Phenomena*. Cambridge University Press, Cambridge, MA(1999).

[7] K. Peng, L. Wang, and J. Slattery, *J.Vac. Sci. Technol. B,* 14, 3317(1996).

[8] Venkat R. Subramanian and Ralph E. White. *Symbolic solutions for boundary value problems using Maple.* Computers & Chemical Engineering 24.11 (2000): 2405-2416.

[9] Thomas F. Fuller, Marc Doyle, and John Newman. *Simulation and optimization of the dual lithium ion insertion cell.* Journal of the Electrochemical Society 141.1 (1994): 1-10.

[10] Daniel A. Scherson and Attila Palencsr.*Batteries and electrochemical capacitors.* The Electrochemical Society Interface Spring 2006.

8 Appendix

- Code for Fig. 1

```
close all
clear all
clc
%Fig. 2 in Mid-term.
%over_1=Ls/kappa_s;
%[7]:
kappa=.138;
kappa_prime=.715;
sigma=20*kappa;sigma_prime=20;
q=1.11;
%\end{verbatim}
%\begin{verbatim}
for x = 1:10
    disp(x)
end
%\end{verbatim}
%\begin{verbatim}
deltaV=.1;
i=.1;
f=0;over_1=0;
syms L
Eq_7=(kappa+sigma)*(deltaV/i-L/(kappa+sigma)-over_1)*q/...
    ((sigma/kappa_prime+kappa/sigma_prime)*(1+f)-1);
Eq_8=q*L;
L_critical=solve(Eq_7==Eq_8);
X1=0:.02:L_critical;
X2=L_critical:.02:1.4;
Eq_7_plot_1=subs(Eq_7,L,X1);
Eq_7_plot_2=subs(Eq_7,L,X2);
Eq_8_plot_1=subs(Eq_8,L,X1);
Eq_8_plot_2=subs(Eq_8,L,X2);
critical_plot=L_critical;
%graphs
plot(X1,Eq_7_plot_1,'--');
hold on
plot(X2,Eq_7_plot_2,'-');
hold on
plot(X1,Eq_8_plot_1,'-');
hold on
plot(X2,Eq_8_plot_2,'--');
y_critical=subs(Eq_7,L,L_critical);
xlabel('L(cm)');
ylabel('$Q(\frac{A-hr}{cm^2})$','Interpreter','LaTex');
text(.2,subs(Eq_7,L,.2)+.2,'Equation [7]');
text(1.1,subs(Eq_8,L,1.1)-.2,'Equation [8]');
hold on
plot([L_critical L_critical],[0 y_critical],'--');
text(double(L_critical)-.1,.1,'Lopt');%Note. text works only for double coordinates.
```

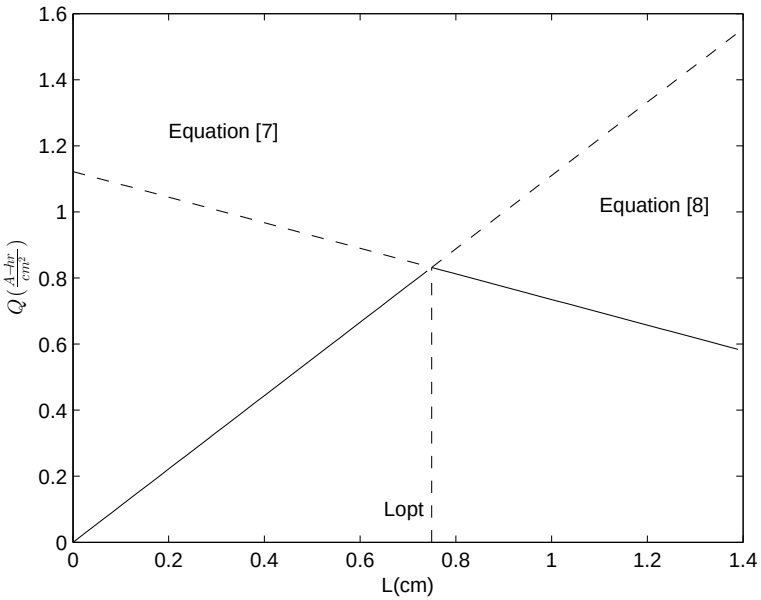

- Code for Fig. 7

```
 % \begin{verbatim}
%reproduceResults_paper.
% %Fig.3, Electrode capacity for various electrode thickness and porousities.
% %Vc=2/3*U;%a reasonable assumption.
% %kappa_s=kappa_0;
%Fig.4, specific energy for various electrode thickness and porosities.
T=100;ratio_sOver0=1;
U=1;
Vc=2/3*U;
%L_plus/Ls----the x-axis, and denotes as ratio_L;
ratio_L=linspace(0,8.5,100);
eps_value=linspace(.1,.7,7);
y=zeros(length(eps_value),length(ratio_L));
C=zeros(length(eps_value),length(ratio_L));
for i=1:length(eps_value)
    eps=eps_value(i);
    %Firstly, compare the three values in [7], [8] and [9] to get the optimal
    %current.
    I_eq7=1/(1+(1+3*ratio_sOver0*T/2*eps^(1.5)*(1-eps))^(1/2));
    I_eq8=2*(1-Vc/U)/(1+(1+4*(U-Vc)*ratio_sOver0*T/(eps^(1.5)*(1-eps)*U))^(1/2));
    I_eq9=ratio_L*(1-eps)/T;
    I=min(I_eq7,I_eq8);
    %disp(I);
    I=min(I,I_eq9);
    C(i,:)=I*T;
    %y----------the dimensionless specific energy to be maximized.
    y(i,:)=((1-I).*I*T-I.^(3)*T^(2)/(2*eps^(1.5)*(1-eps))./...
    (1+ratio_L);
end
plot(ratio_L,y);
%\end{verbatim}
\includegraphics [width=4in]{paper2_fig3_01-eps-converted-to}
```

- Code for Figs. 9 and 10.

```
clear all
clc
%codes_paper3
```

```
%Fig.2. Measured capacity loss and estimated SEI
%thickness as functions of time and temperature for HE prototype cells
%stored a float potential of 3.9v.
z_p=2;%stoichiometric coefficient
c_p=2.11*1e6/74;
c_eq=2.636e3;
A_anode=173;
%lambda=.21168;
D_s=[3.07;15.1].*1e-23;
N_0=[50.93;49.16].*(3600);%initial capacity.
F=9.6485e4;
sqrt_t=linspace(0,22,100);
x=zeros(length(D_s),length(sqrt_t));
l=zeros(length(D_s),length(sqrt_t));
syms y
lambda=solve((sqrt(pi)*c_p)*y-c_eq*exp(-y^2)/erf(y),y);
%lambda=lambda/1000;
%return
%lambda=.211;
for i=1:length(D_s)
  x(i,:)=F*2*z_p*c_p*A_anode*lambda*sqrt(D_s(i))*(sqrt_t)*sqrt(3600*24)*100/N_0(i);
    l(i,:)=2*lambda*sqrt(D_s(i))*(sqrt_t)*sqrt(3600*24)*1e9;
end
 [ax,h1,h2] =plotyy(sqrt_t,x,sqrt_t,l);%fig_paper3
 set(ax(1),'YLim',[0 20]);
 set(ax(2),'YLim',[0 36.5]);
 figure
plot((sqrt_t).^2,x);%1_paper3
axis([0 100 0 9])
figure
plot((sqrt_t).^2,100-x);%2_paper3
axis([0 100 91 100])
\includegraphics [width=4in]{paper3_all_01-eps-converted-to}
\includegraphics [width=4in]{paper3_all_02-eps-converted-to}
\includegraphics [width=4in]{paper3_all_03-eps-converted-to}
```

- Codes for dendrite problem.

The following are codes for the last section 5.
Firstly, we need to define the parameter for Lithium batteries in a parallel-electrode lithium/polymer cell.

```
D=[5e-12];       %Salt diffusion coefficient, m^2/s
tpluss=0.3;      %cation transference number
Cb=1000;         %initial bulk concentration of lithium salt, mol/m^3
L=100*10^(-6.0);          %interelectrode distance, m
F=96487;          %Faraday constant
R=8.3143;         %ideal gas constant
cref=1000;       %reference concentration, mol/m^3
T=358.15;         %Temperature, K
IL= -2.0*Cb*D(1)*F/(1.0-tpluss)/L;       %Limiting current
I=0.95*IL;       %current density
V=1.2998*10^(-5);        % molar volume of lithium, m^3/mol
gamma = 1.716;  %surface energy, J/m^2
lambda = F*F*D(nn)/(2*tpluss*(1-tpluss)*R*T);    %equivalence cond, Sm^2/mol
```

The following steps lead to concentration profile Fig.11.

```
t=exp([1 2 3 4 5 6 7]);
x=(0.0:L/25:L);
N1=size(t,2)
figure(2)
for i=1:N1
        plot(x,concentration(x,t(i),I,D(nn),tpluss) ,'b');
```

i	Time (s)
$0.95i_L$	8050
$0.5i_L$	$4.209\text{x}10^4$
$0.05i_L$	$5.27\text{x}10^5$

Table 1: Time short out for limiting current

```
        hold on
end
```

Codes for potential profile Fig.12,

```
figure(3)
for i=1:N1
plot( x ,potential3(x,t(i),I,lambda,R,T,F,tpluss));
hold on;
grid on;
end
```

Codes for Fig.15,

```
tt1=[(0:5:500)];
N1=size(tt1,2);
N2=size(x,2);
[TT XX]=meshgrid( tt1 , x);
rr=(0.0:L/100*0.1:L*0.3);
N3=size(rr,2);
for kk=1:N3
        for ii=1:N2
            for jj=1:N1
                ZZ(ii , jj)=VelocityTip( x(ii) , tt1(jj) , I , lambda , R ,
                T , F , tpluss  , gamma , V , rr(kk) ,D(nn)  );
            end
            [Imax(ii) indexR ]=max(ZZ(ii));
        end
        clear ZZ;
        [IImax(kk) IndexRadiu ]= max( Imax );
end
[IIimax IndexRadiusF ]=max(IImax);
display('radius=');
display(rr(IndexRadiusF));
```

for time fixed $t = 1900s$, we can get Fig.13 using the following codes,

```
for i=1:N2
vsol2(i)=Velocitytip(x(i) , 1900, I , lambda , R , T , F ,
 tpluss  , gamma , V , rr(IndexRadiusF)  ) ;
end
figure(7)
plot(x , vsol2 )
```

Using Runge Kutta in matlab (ode45), we can obtain Fig.14,

```
[Tsol Ysol ]=ode45( @(tt , yy )Velocitytip( yy , tt , I , lambda , R , T ,
        F , tpluss  , gamma , V , 1.0e-7 ,D(nn) ) , [0 8050] , [0] );
figure(5)
plot(Tsol , Ysol);
```

The following are the assistant function for the above main files.

```
function [y] = THETAstadystate( xi  )
% input xi = Distance dimensionaless
% output y Solution stady State
        y= -1.0*xi+1/2.0;
end
```

```
function [y] = THETAtransient( xi , tao , N )
% Input xi: Distance dimensionaless
%       tao: Time dimensionaless
%       N: # termins for Fourier series
% output y Solution transient state
        temp=0.0;
        for j=1:N
        temp1 = 2.0*j-1.0;
        temp1=temp1*pi;
        temp=temp+1.0/(temp1^2)*(exp(-1.0*(temp1^2.0)*tao))*cos(temp1*xi);
        end
        y = -4.0*temp;
end

function [y] = concentration( x , t  , I , D , tpluss)
% input x: distance (m)
%       t: time (s)
%       I: Current density (A/m^2)
%       D: diffusion coeficient (m^2/s)
%       tpluss: cation transference number
% output y: concentration (mol/m^3)
        F=96487; %(C/mol)
        L=100e-6.0; % Distance Ref (m)
        Cb=1000; % initial concetration (mol/m^3)
        xi = x/L;
        tao=D*t/L/L;
        y =(THETAstadystate(xi)+THETAtransient(xi,tao,20))*(1.0-tpluss)*I*L/D/F
                                                                          +Cb;
end

function y = overpotentialS( x , t ,T , I , F , R ,D , tpluss )
% input x: distance (m)
%       t: time (s)
%       T: Temperature (K)
%       I: current Density (A/m^2)
%       F: Faraday's constant
%       R: Ideal gas constant
%       D: diffusion coeficient (m^2/s)
%       tpluss: cation transference number
% output y: overpotential (v)
        i0=-30.0 ; %current reference
        cref=1000; % concentration reference
        [y] = 2*R*T/F*asinh( 0.5* (I/i0)*
         (cref/concentration( x , t , I , D , tpluss)).^0.5 );
end

function [y] = potential3( x , t , I , lambda , R , T , F , tpluss ,D )
% input x: distance (m)
%       t: time (s)
%       I: current Density (A/m^2)
%       lambda: equivalent conductance (Sm^2/mol)
%       R: Ideal gas constant
%       T: Temperature (K)
%       F: Faraday's constant
%       tpluss: cation transference number
%       D: diffusion coeficient (m^2/s)
% output y: potential3 (v) potential in vicinity of dendrite tip
        N1=size(x,2);
        for i=1:N1
        pp=(0.0:x(i)/100:x(i));
            cc=trapz( pp , 1./concentration(pp,t,I , D ,tpluss) );
        y(i) = overpotentialS( x(i) , t , T , I , F , R ,D , tpluss );
        y(i)= y(i)-I/lambda * cc;
        y(i)=y(i)+R*T/F*(1-2*tpluss)*log( concentration(x(i),t,I ,D ,tpluss)
```

```
                    /concentration(0,t,I,D , tpluss) );
            end
        end

function [ y ] = dendritePotential( x,t,I,lambda,R,T,F,tpluss,gamma,V,r,D)
        % input x: distance (m)
        %        t: time (s)
        %        I: current Density (A/m^2)
        %        lambda: equivalent conductance (Sm^2/mol)
        %        R: Ideal gas constant
        %        T: Temperature (K)
        %        F: Faraday's constant
        %        tpluss: cation transference number
        %        D: diffusion coeficient (m^2/s)
        % output y: potential3 (v) potential in vicinity of dendrite tip
            y= potential3( x , t , I , lambda , R , T , F , tpluss ,D );
        end

        function [ y ] = currentNormal( x,t,I,lambda,R,T,F,tpluss,gamma,V,r,D)
        % input x: distance (m)
        %        t: time (s)
        %        I: current Density (A/m^2)
        %        lambda: equivalent conductance (Sm^2/mol)
        %        R: Ideal gas constant
        %        T: Temperature (K)
        %        F: Faraday's constant
        %        tpluss: cation transference number
        %        gamma surface energy (J/m^2)
        %        V: molar Volumen of lithium
        %        D: diffusion coeficient (m^2/s)
        % output y:  current density normal to dendrite (A/m^2)
            cref=1000; %concentration refence
            i0=-30.0;  % current refence
            eta=-1.0*dendritePotential( x,t,I,lambda,R,T,F, tpluss , gamma, V ,r ,D);
            temp1=exp(2*gamma*V/r/R/T);
            temp2=exp(0.5*F.*eta/R/T);
            temp3=exp(-0.5*F.*eta/R/T);
            % cc=concentration for x and t
            cc=concentration( x , t  , I , D , tpluss);
            temp4=-1.0*(1-tpluss)*r*i0.*temp3/F/D./cc;
            y=i0*(temp1*temp2-temp3)./( (cref./cc).^0.5+temp4);
        end

        function [ y ] =VelocityTip( x,t,I,lambda,R,T,F,tpluss,gamma,V,r,D)
        % input x: distance (m)
        %        t: time (s)
        %        I: current Density (A/m^2)
        %        lambda: equivalent conductance (Sm^2/mol)
        %        R: Ideal gas constant
        %        T: Temperature (K)
        %        F: Faraday's constant
        %        tpluss: cation transference number
        %        gamma surface energy (J/m^2)
        %        V: molar Volumen of lithium
        %        D: diffusion coeficient (m^2/s)
        % output y:  Velocity tip (m/s)
            y = 1.0*V/F*currentNormal( x , t,I,lambda,R,T,F,tpluss,gamma,V,r,D);
        end
```

9 List of symbols

Table 2: Section 2

Q	$\triangleq$	electrode capacity, $A-s/cm^2$
i	$\triangleq$	current density, A/cm^2
t	$\triangleq$	time, s
L	$\triangleq$	electrode thickness, cm
q	$\triangleq$	effective electrode capacity equal to $q_0(1-\epsilon)$, $A-s/cm^3$
ΔV	$\triangleq$	voltage loss, V
$R_{(i,t)}$	$\triangleq$	resistance, ohm/cm^2
L_s	$\triangleq$	separator thickness, cm
κ_s	$\triangleq$	conductivity of the separator, mho/cm
κ	$\triangleq$	effective conductivity of solution in porous matrix in the charged state, mho/cm
σ	$\triangleq$	effective conductivity of the solid phases in the porous matrix in the charged state, mho/cm
κ'	$\triangleq$	effective conductivity of solution in porous matrix in the discharged state, mho/cm
σ'	$\triangleq$	effective conductivity of the solid phases in the porous matrix in the discharge state, mho/cm
f	$\triangleq$	fraction increase in electrode thickness due to volume changes
κ_0	$\triangleq$	conductivity of the bulk solution, mho/cm
σ_0	$\triangleq$	conductivity of the bulk solid phases in the charged state, mho/cm
ϵ	$\triangleq$	electrode porosity in the charged state
n	$\triangleq$	a parameter which accounts for tortuosity effects
ϵ_f	$\triangleq$	electrode porosity in the discharged state
σ_0'	$\triangleq$	conductivity of the bulk solid phases in the discharged state, mho/cm
q_0	$\triangleq$	specific electrode capacity, $A-s/cm^3$
B	$\triangleq$	a parameter which accounts for volume changes within the electrode

Table 3: Section 3

V	$\triangleq$	cell potential, V
U	$\triangleq$	open-circuit potential, V
i	$\triangleq$	superficial current density, A/cm^2
I	$\triangleq$	dimensionless current density
L_+	$\triangleq$	thickness of positive electrode, cm
L_s	$\triangleq$	thickness of the separator, cm
L_r	$\triangleq$	thickness of residual parts, cm
M	$\triangleq$	mass per unit separator area, g/cm^2
q_+	$\triangleq$	capacity density of solids in the positive electrode, C/cm^3
q_-	$\triangleq$	capacity density of the negative electrode, C/cm^3
t	$\triangleq$	time, s
t_d	$\triangleq$	discharge time, s
T	$\triangleq$	$U\kappa_s t_d/q_+ L_s^2$
V_c	$\triangleq$	cutoff potential, V
ϵ	$\triangleq$	electrode porosity
κ	$\triangleq$	electrolyte conductivity in positive electrode, S/cm
κ_0	$\triangleq$	inherent electrolyte conductivity, S/cm
κ_s	$\triangleq$	conductivity of separator, S/cm
ρ_+	$\triangleq$	average density of the positive solid material, g/cm^3
ρ_-	$\triangleq$	density of the negative electrode, g/cm^3
ρ_r	$\triangleq$	average density of residual parts, g/cm^3
ρ_s	$\triangleq$	density of the electrolyte, g/cm^3

Table 4: Section 4

S	$\triangleq$	solvent species
P	$\triangleq$	solvent reduction product
R	$\triangleq$	gas constant, $cal/molK$
L	$\triangleq$	SEI thickness, cm
L_0	$\triangleq$	initial SEI thickness, cm
c	$\triangleq$	total molar concentration of the SEI phase, mol/com^3
c_{eq}	$\triangleq$	equilibrium solvent molar concentration, mol/com^3
c_P	$\triangleq$	product molar concentration in the SEI phase, mol/com^3
c_S	$\triangleq$	solvent molar concentration, mol/com^3
u	$\triangleq$	similarity transformation variable
Z_P	$\triangleq$	the stoichiometric coefficient of Li in P
x	$\triangleq$	fractional capacity loss
N_0	$\triangleq$	the initial number of moles of lithium available
A_{anode}	$\triangleq$	the anode area,cm^2
D_S	$\triangleq$	solvent diffusivity in the SEI phase, cm^2/s

Table 5: Section 5

c_b	$\triangleq$	initial bulk concentration of lithium slat, mol/m^3
c_{ref}	$\triangleq$	reference concentration of lithium salt, mol/m^3
D	$\triangleq$	salt diffusion coefficient, m^2/s
F	$\triangleq$	Faraday's constant, 96487 C/mol
I	$\triangleq$	current, A
R	$\triangleq$	ideal gas constant, 8.3143 $J/molK$
r	$\triangleq$	dendrite tip radius, m
θ	$\triangleq$	$(c - c_b)DF/(1 - t_+^0)iL$ dimensionless concentration
ξ	$\triangleq$	dimensionless distance
τ	$\triangleq$	dimensionless time
η_S	$\triangleq$	surface over-potential, V
γ	$\triangleq$	surface energy, J/m^2
Φ_3	$\triangleq$	potential in vicinity of dendrite tip, V
i	$\triangleq$	current density, A/m^2
Λ	$\triangleq$	$F^2D/t_+^0(1 - t_+^0)RT$ equivalent conductance, Sm^2/mol
κ	$\triangleq$	electrolyte conductivity, S/m
κ_a	$\triangleq$	anodic rate constant
κ_c	$\triangleq$	cathodic rate constant
T	$\triangleq$	absolute temperature, K
α_a	$\triangleq$	anodic transfer coefficient
α_c	$\triangleq$	cathodic transfer coefficient
v_{tip}	$\triangleq$	dendrite propagation velocity m/s
y_{tip}	$\triangleq$	dendrite tip position, m
t	$\triangleq$	time, s
t_s	$\triangleq$	time passed before cell failure, s
t_+^0	$\triangleq$	cation transference number
Q	$\triangleq$	charge passed per unit area, C/cm^2
Q_s	$\triangleq$	charge passed per unit area before cell failure, C/cm^2
L	$\triangleq$	interelectrode distance, m
i_L	$\triangleq$	$2c_bDF/(1 - t_+^0)L$ limiting current density, A/m^2
i_n	$\triangleq$	current density normal to dendrite tip, A/m^2
V_0	$\triangleq$	open-circuit potential, V